Assessment of Performance Degradation of the Spacesuit Water Membrane Evaporator (SWME) Materials Due to Environmental Conditions

Morgan B. Abney[1] and Sara Wilson[2]
NASA Engineering & Safety Center, Hampton, VA 23681

Ray Pitts[3]
NASA Kennedy Space Center, Cape Canaveral, FL 32815

Elspeth Petersen[4]
NASA Johnson Space Center, Houston, TX 77058

Dibakar Bhattacharyya[5]
University of Kentucky, Lexington, KY 40506

Glenn Lipscomb[6]
University of Toledo, Toledo, OH 43606

and

James Reeder[7] and John Steele[8]
TEAMS3, Langley Research Center, Hampton, VA 23681

The Spacesuit Water Membrane Evaporator (SWME) is a next-generation design to replace the sublimator in spacesuits for thermal control. The SWME design includes nearly 28,000 hollow fiber membranes epoxied into a titanium housing. Limited data are available to understand the risk of exposure of the SWME materials to nominal and off-nominal conditions including organic chemicals, inorganic chemicals, particulates, and microbes. This effort sought to empirically investigate the effects of changing membrane characteristics such as pore size, porosity, and surface energy on membrane performance and the effects of environmental conditions on those characteristics. Performance data are presented and the long-term impacts on SWME performance are discussed. Effects of broken fibers, crimped or crushed fibers, and changes in fiber surface energy are also explored.

Nomenclature

EVA	=	Extravehicular Activity
ISS	=	International Space Station
LCVG	=	Liquid Cooling and Ventilation Garment
PLSS	=	Portable Life Support System
ppm	=	parts per million
SWME	=	Spacesuit Water Membrane Evaporator

[1] ECLSS Technical Fellow, NESC C104, MSFC, AL 35812.
[2] Statistician, NASA Engineering and Safety Center, C102, NASA Langley Research Center, Hampton, VA 23666
[3] ISRU Research Engineer, Exploration Research and Technology, and Mailstop UB-E00, Cape Canaveral, FL 32899
[4] Air Revitalization Research Engineer, Crew and Thermal Systems, and 2101 E NASA Pkwy, Houston, TX 77058
[5] Professor, Chemical Engineering, University of Kentucky Center of Membrane Sciences, 351 Ralph G Anderson Building, Lexington, KY 40506
[6] Professor, Chemical Engineering, School of Green Chemistry and Engineering, MS 305, 2801 W Bancroft St, Toledo, OH 43606.
[7] Research Engineer, Durability, Damage Tolerance and Reliability Branch, NASA Langley, M/S188E, Hampton, VA 23666
[8]Subject Matter Expert, MRI Technologies, 17047 El Camino Real, Suite 200, Houston, TX 77058

I. Introduction

MAINTAINING controlled temperature of a crew member and their portable life support system (PLSS) during extravehicular activity (EVA) is a critical capability for space suit designs. Space suits used for EVA on the International Space Station (ISS) employ a water cooling loop that circulates through both the Liquid Cooling and Ventilation Garment (LCVG) to provide cooling to the crew member and through the PLSS. The ISS PLSS sublimator, as shown Figure 1, is made up of steel plates in which pressurized liquid water enters one side, freezes, and is then sublimated to space vacuum on the other side of the plate to provide cooling. While ISS sublimators have proven generally reliable and have exceeded their original design life, they are challenging to manufacture and cannot be used on the surface of Mars where the atmospheric pressure is greater than the triple point of water. For these reasons, NASA initiated development of the Spacesuit Water Membrane Evaporator (SWME) for the Exploration Extravehicular Mobility Unit (xEMU).[1-5] The design was provided to suit vendors as part of the Exploration Extravehicular Activity Services (xEVAS) contracts.[6]

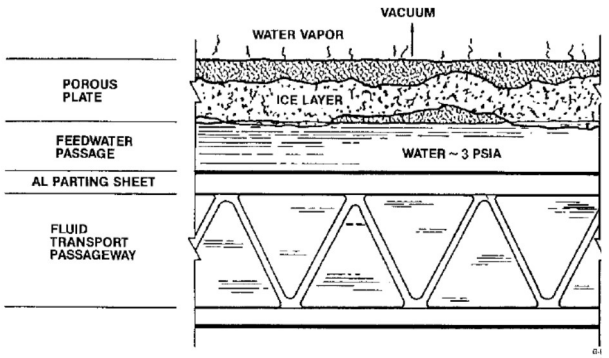

Figure 1. Sublimator design used in the ISS PLSS.

The SWME is designed to provide cooling to the circulating water via evaporation through hydrophobic hollow fiber membranes. The SWME assembly is comprised of three modules, each containing ~9300 hollow fiber membrane tubes. During operation, water flows through the inside of the hydrophobic hollow fibers (lumen side). Vacuum is applied to the outside of the fibers (shell side). Pores in the wall of the fibers allow water vapor to pass through the fiber wall to vacuum shell side, thereby cooling the circulating water. The hydrophobic nature of the tubes and proper pore size distribution helps prevent liquid water from passing through the pores. During development, several studies were conducted to optimize the form factor, size, and scale of the SWME[1], to design a valve that would allow for crew temperature control[2], to evaluate short-term contamination exposure[3,4], and to evaluate the effects of long-duration operation[5].

While the results of these studies were data demonstrating acceptable operational performance of the SWME under nominal and limited off-nominal conditions, a key consideration that must be addressed prior to flight is how the SWME might degrade and/or fail during EVA in the space environment. Further, once failure mechansims have been identified, it is critical that the failures are characterized such that early detection is possible and operational responses can be implemented in time to protect the crew.

In response to this gap in knowledge, potential failure mechanisms of the SWME were identified at the assembly, the module, and the membrane levels. At the assembly level, a key concern was the effect of vibration from both launch and landing loads and the prolonged and intermittent vibrations associated with surface activities during EVA on the Lunar or Martian surfaces (e.g. traversing the surface, falling down, riding in a rover, etc). At the SWME module level, a key concern was failure of the epoxy that holds the hollow fiber membranes in the SWME housing. Finally, at the hollow fiber membrane level several adverse effects were identified including: chemical contamination, biological contamination, and mechanical damage to the fibers (crimps in the fibers, cuts in the fibers, and changes in the surface energy of the fibers). Once identified, testing was conducted to evaluate each failure mechanism. A complimentary effort is underway to model and to quantify the conditions leading to these failures with the intention of using the model to provide real-time monitoring of SWME health, to provide early detection of SWME degradation, and to predict the remaining lifetime of individual SWME assemblies during EVA on the Lunar or Martian surfaces[7]. Here we report the results of failure mechanism testing and conclusions drawn to-date.

II. Materials and Methods

Four tests were designed to evaluate the identified failure mechanisms. The first consideration for evaluating failures at the membrane level was to understand how changes to the membrane affected thermal performance. Critical characteristics of the hollow fiber membrane and their influence on thermal performance were evaluated as described in Section A below. Next, SWME hollow fiber membranes were exposed to organic, inorganic, and biological contaminants at varying levels to characterize their effect on thermal performance. The specifics of the contaminant exposure testing are described in Section B below. Defect and mechanical damage testing was then performed to

evaluate their effects on thermal performance as described in Section C below. Finally, vibration testing was conducted at the assembly level but will be described in a future paper.

A. Critical Characteristic Testing Materials and Methods

The thermal cooling performance of the SWME hollow fiber membranes is known to be affected by several critical membrane characteristics including the membrane pore diameter (d_p), the membrane porosity (φ_p), the thickness of the membrane tube walls (δ), the tortuosity of the pores in the membrane (τ), and the surface energy (hydrophobicity) of the inner wall of the tubes. Changes to these characteristics will affect the heat rejection performance (Watts) of the SWME to varying levels. Mathematical modeling of hollow fiber membranes used in a SWME architecture was described by Kahn *et al.*[7] The derivation shows that heat rejection per unit length can be described as shown in Equation 1,

$$Q = \int_{z=0}^{L} \lambda_v J_k \pi d_l dz \qquad \text{Eq. 1}$$

where Q is the heat rejection in Watts/m, λ_v is the latent heat of vaporization of water in J/kg, J_k is the mass flux of vapor through the pores (by Knudsen diffusion) in kg/m^2/s, d_l is the inner diameter of the lumen in meters, and L is the length of the tubes in meters.The mass flux of vapor can be further derived as shown in Equation 2,

$$J_k = (0.0248) S_p \sqrt{\frac{1}{T_p}} (\Delta P) \qquad \text{Eq. 2}$$

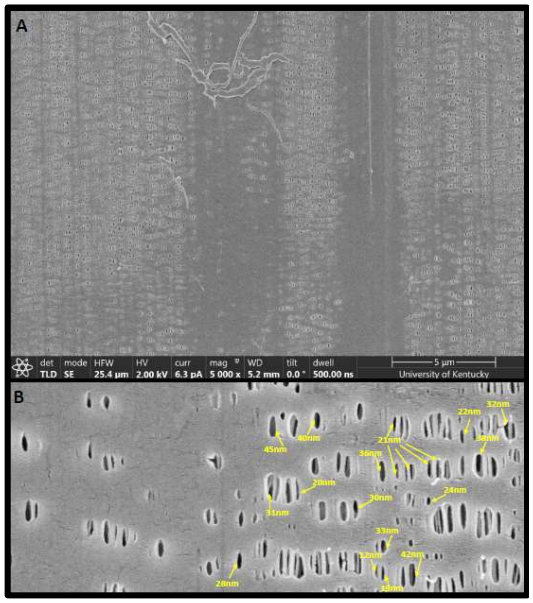

Figure 2. Scanning electron microscope image of Membrane B shell side surface (platinum coated).

where $S_p = \frac{d_p \phi_p}{\delta \tau}$ and is termed the overall membrane structure parameter, T_p is the pore mouth temperature at a given pore along the length of a membrane tube, ΔP is the pressure drop across the membrane (P_{vapor}-P_{shell}) at the pore liquid-gas interface, P_{vapor} is the water vapor pressure at T_p, and P_{shell} is the specified shell pressure. An approximate algaebraic solution for the entire membrane can then be determined by assuming an average temperature ($T_{ave} = \frac{T_{in}+T_{out}}{2}$, where T_{in} is the lumen inlet temperature and T_{out} is the lumen outlet temperature) and estimating $(P_{vapor})_{ave}$ and $(\lambda_v)_{ave}$ to calculate $(J_k)_{ave}$ and $(Q)_{ave}$. The overall membrane structure parameter is a constant for a given membrane. Observed changes in heat rejection under identical conditions can then indicate changes to the critical characteristics and can signal inherent changes to the membrane (i.e. failure modes).

Validation of the model requires empirical data showing the quantified effects of changes to the critical characteristics on performance. To accomplish this, three unique hollow fiber membranes were identified for testing. All of the membranes were constructed from the same polymer. Due to the proprietary nature of the materials, they are described here as membranes A, B, and C. The critical characteristics of each hollow fiber membrane tested, both reported by the vendor and as measured in this effort, are shown in Table 1. A scanning electron microscope image of Membrane B is shown in Figure 2.

Table 1. Critical characteristics of hollow fiber membranes (vendor reported/experimentally determined).

Membrane	Tube Inner Diameter (µm)	Wall Thickness (µm)	Pore Size Ave (nm)	Porosity (%)
A	200/200	50/48	30/39	25/18
B	220/217	40/43	40/38	40/28
C	200/204	50/46	ND/38	ND/15

1. Critical Characteristic Test Matrix

A test matrix was developed to test the three membranes across three factors in a randomized run order. The three factors considered included water flow rate through the lumen, water inlet temperature, and shell pressure as shown in Table 2. Level 2 for water flow rate and water inlet temperature are consistent with the expected values in SWME during an EVA with flow adjusted to reflect module size and number of membranes. The shell pressure was expressed as a percentage of the vapor pressure calculated from the inlet temperature. For Lunar surface EVA, the available vacuum pressure will be very low. Level 1 of the shell pressure was set as low as reasonably achievable (ALARA) with the available vacuum pump (ALARA = 1.1-16 torr). For Martian surface EVA, the available pressure is 5-7 torr, which is consistent with Level 2 shell pressure for the expected lumen inlet water temperature during EVA. The inlet pressure is maintained constant at 165.5 kPa (24 psia). During testing, each set of conditions was maintained for 5-30 minutes after steady state was reached (based on the engineering judgement of the test conductor).

Table 2. Critical characteristic test matrix.

Factor	Level 1	Level 2	Level 3
Lumen Water Flow Rate [mL/min]	18	32.7	44.7
Lumen Water Inlet Temperature [C]	5º	19º	30º
Shell Pressure	ALARA	40%	70%

2. Critical Characteristic Test Fixture Description

Sub-scale modules were fabricated in-house at NASA with each of the hollow fiber membranes, as shown in Figure 3. Each module was fabricated with ~600 tubes of 11.9 cm (4.7 in) length (shown in white in Figure 3). The tubes were bonded to a standard KF40 vacuum flange ring with custom seats (silver in the image) using epoxy (orange in the image). Stiffiners (vertical silver bars in the image) were added to the assembly to prevent bending of the fibers during handling. The sub-scale modules were installed into a KF40 cross for testing in the Thermal Performance Test Stand.

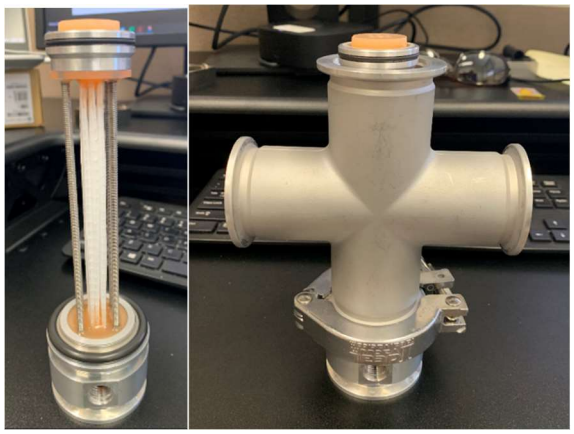

Figure 3. Critical characteristic sub-scale module (left) and test assembly (right).

3. Thermal Performance Test Stand Description

The Thermal Performance test stand was designed to evaluate heat rejection performance of various test fixtures. Apache stainless steel tanks were used for feed water (Tank 1) and waste water (Tank 2) such that the source water was always fresh. This prevented cross-contamination between test articles and between the two test stands. Each tank was placed on a scale to provide secondary measurement of water usage. An Alicat liquid flow controller was used to control water flow to the test fixture. A heat exchanger connected to a water chiller/heater was used to control the inlet temperature of the water. Fluke 5665-B immersion probe thermistors were used to measure the temperature in Tank 1, at the fixture lumen inlet, at the fixture lumen outlet, in the vacuum line, and in the ambient environment. Hand valves were used throughout the system for isolation. Two sensors were used to measure pressure on the shell side of the test stand including an Inficon Pirani Standard Gauge Model PSG502-S pressure transducer and an MKS Capacitance Manometer Model DA02A. A Scroll Labs SVF-E2-100 floating scroll pump was used to provide vacuum. A Cascade 3-Quart Dry Ice Cold Trap was placed between the test fixture and the vacuum pump to collect water vapor. A mixture of isopropyl alcohol and dry ice was used to cool the cold trap during testing.

Custom Labview software was designed to control the flow controller and to record data from the scales, the flow controller, the thermistors, and the pressure transducer. All other data was recorded manually during testing and stored in the Labview notes function and in Onenote.

B. Contamination Testing Materials and Methods

Long-term use of hollow fiber membranes in industry has identified failures related to contamination, particularly biological contamination and particulates. Flight experience with the ISS sublimator revealed potential concerns with water quality[8]. Ongoing flight experiments on ISS provided data on known flight water quality in a similar system[9]. These lessons learned provided a chemical basis for the ersatz solution used in the contamination testing.

1. Contamination Test Matrix and Test Fixtures

Three categories of contaminants were identified for evaluation including organic, inorganic, and biological. For organic and inorganic contaminants, ersatz solutionswere developed as shown in Table 4 and concentrated to two levels: one at a level consistent with recycling in the PLSS recirculation loop after 25 EVAs (Medium) and a second level consistent with 50 EVAs (High). Two microbial mixtures containing *S. sanguinis*, *C. metallidurans*, *R. insidiosa*, and *M. fujisawaense* were also developed. For the Medium and High levels of organics, concentrations of 1.25E+05 and 3.80E+05 colony forming units per milliliter (CFU/mL) were targeted, respectively. Iodine, which can change the surface chemistry of (oxidize) the polypropylene fibers, was included as a biocide at 2 parts per million (ppm) for the Medium level and 4 ppm for the High level at the start of each test, but was not re-dosed during testing. A "Low" level of any of the the contaminants meant that none of the contaminants in that category were present in the ersatz. Statistical design of experiments was used to define 28 tests with varying levels of each category of contaminant as shown in Table 3. Conductivity and pH measurements were taken at the beginning of all tests and approximately every 3 days. A Cole Parmer PC200 pH/conductivity meter was used to measure both pH and conductivity. A three-point pH calibration (pH 4, 7, and 13) and a two-point conductivity calibration (12.88 uS/cm and 1413 uS/cm) were performed each day before use and corrected to a laboratory temperature of 20ºC.

Table 3. Contamination test matrix.

Test Run #	Inorganic	Organic	Biocide
1	High	Medium	Low
2	Low	Medium	Low
3	Medium	Medium	Low
4	Medium	Medium	Low
5	Medium	Low	Low
6	Medium	High	Low
7	Low	High	Low
8	Medium	Medium	Low
9	Medium	Medium	Low
10	High	High	Low
11	High	High	Low
12	Low	High	Low
13	High	Low	Low
14	Low	Low	Low
15	Medium	Medium	Low
16	Low	Low	Low
17	High	Low	Low
18	Low	Medium	Low
19	Low	Medium	Medium
20	Medium	Medium	Medium
21	High	High	High
22	Medium	Medium	Medium
23	High	Medium	Medium
24	Medium	High	Medium
25	Medium	Low	Medium
26	Low	Low	High
27	High	Low	High
28	Low	High	High

Table 4. Ersatz contaminant target concentrations.

Chemical Name	Chemical Formula	Target concentrations in ersatz soln (mg/L)		
		Low	Medium	High
Potassium Iodide	KI	0	18.5	55.5
Sodium Chloride	NaCl	0	3.9	11.7
Nickel(II) acetate tetrahydrate	$C_4H_6NiO_4$	0	1.44	4.3
Sodium Metasilicate Nonahydrate	$Na_2O_3Si \cdot 9H_2O$	0	8.85	26.6
Ammonium Carbonate	$(NH_4)_2CO_3$	0	4.68	14.0
Iron Chloride Hexahydrate	$FeCl_3$-$6H_2O$	0	5.07	15.2
Trimethylsilanol	$C_3H_{10}OSi$	0	6.82	20.5
N-n-Butylbenzene sulfonamide	$C_{10}H_{15}NO_2S$	0	0.38	1.1
2-Hydroxybenzothiazole	C_7H_5NOS	0	0.5	1.5
1,3,5-triallyl-1,3,5-triazine-2,4,6 (1H, 3H, 5H) trione	$C_{12}H_{15}N_3O_3$	0	0.8	2.4
Bisphenol-A	$C_{15}H_{16}O_2$	0	60.8	182.5
Acetic Acid	CH_3COOH	0	12.2	36.5

Commmercially available hollow fiber membrane cartridges containing the membranes used in SWME were purchased and used for all contamination testing. Each cartridge contains approximately 1200 fibers of ~14.5 cm (5.7 in) in length. Prior to contamination testing, each cartridge was installed in the Thermal Performance Test Stand (described in Section A.3) to establish baseline heat rejection performance. The cartridge was then exposed to contaminants in the Recirculation Test Stand (described below) for a period of 6-9 days. At that point, it was removed from the Recirculation Test Stand and installed in the Thermal Performance Test Stand for a "performance check." The cartridge was then returned to the Recirculation Test Stand for the remainder of the testing and removed on day 19 or 20 of testing for a final performance check in the Thermal Performance Test Stand.

2. Recirculation Test Stand

The Recirculation Test Stand was designed to expose each cartridge to targeted contaminants as if they were in-use during an EVA. A total of 10 loops were constructed with each loop designed to test a single cartridge at one time. Two Scroll Labs floating scroll pumps were used (one on loops 1-5, and the other on loops 6-10) to provide vacuum to the shell side of the cartridges at ALARA pressure. Water vapor was not collected with a cold trap in the vacuum lines, rather was pumped out to the laboratory via the floating scroll pump. Contaminant water was stored for each loop in a carboy with a stir bar and recirculated using a peristaltic pump at 125 mL/min to mimic the flow per fiber seen in the SWME. Thermocouples were used to measure the temperature of the water entering and exiting the cartridges. Line heaters were used to heat the inlet water to a temparture of 19ºC. A custom Labview program was designed to control the heaters and capture data from the thermocouples. All other components of the system were manually controlled. Water samples were taken at ~4 day intervals during testing.

3. Modified Thermal Performance Test Stand

Two changes were made to the Thermal Performance Test Stand during contamination testing. First, due to the integration of cartridges in place of the Critical Characteristic Test Fixture, the vacuum pressure transducer was moved to the vacuum line (rather than the opposite leg). Second, the cold trap was not cooled during cartridge testing.

Both the thermal performance baseline test of each cartridge and the "performance checks" were conducted with a water flow rate of 50 mL/min and an inlet temperature of 19ºC. Vacuum pressure was maintained ALARA (3.2-8.4 torr).

C. Defect and Mechanical Damage Testing Materials and Methods

The goal of this testing was to evaluate how defects and mechanical damage affected thermal performance of the SWME membranes. Crimp testing evaluated the effects of "crimps" where a SWME module may have been damaged through handling or physical contact with another surface that could cause partial occlusion of the fibers. Cut testing sought to evaluate the change in performance as a function of the number of ruptured fibers in a module. Hydrophobicity testing was designed to evaluate the effects of changing surface energy (contact angle) of the membrane on thermal performance. Any surfactant exposure to the hollow fiber membrane is known (through internal and industry experience) to decrease hydrobicity and cause "weeping" of the fibers where liquid water is able to pass through the pore of the membranes. Since liquid water entry pressure from the lumen to the pores is directly proportional to cosine (contact angle)[7], any lowering of this value due to surface active agents will lower the weeping pressure and thus increase the risk of potential failures. Each test is described below.

1. Defect and Mechanical Damage Test Matrix

The defect test matrix shown in Table 5 included at least two or three runs of each of the tests described below to provide data with replicates. All the tests used custom made modules (identical to those used in Critical Characteristics testing) assembled with the hollow fiber membrane Material B. With the exception of Cut Testing, all defect tests were conducted with new (unused) modules. Cut testing reused modules from Critical Characteristics testing as described.

Table 5. Master test matrix for SWME fiber defect testing.

Cartridge #	Defect Type	Defect Levels Tested per Cartridge
1	Crimp fibers	0, 5, 10, 20, 50 fibers
2	Cut fibers	0, 1 fibers
3	Cut fibers	0, 1 fibers
4	Decrease in hydrophobicity	2 levels of surfactant
5	Crimp fibers	0, 5, 10, 20, 50 fibers
6	Decrease in hydrophobicity	2 levels of surfactant
7	Crimp fibers	0, 5, 10, 20, 50 fibers
8	Decrease in hydrophobicity	1 level of surfactant

a. Crimp Testing Description

Crimp testing was conducted by first performing a Baseline Performance Check to document the performance of the module with no modifications. The module was then removed from the test stand and place under a Zeiss SteREO Discovery V8 optical microscope, KL 2500 with LCD Lights. Using a magnification of 1.25x, Peer Vigor Swiss Stainless Steel #5 Tweezers were used to pinch the desired number of fibers. Note that the fibers were pinched one at a time and held with sufficient force to just flatten the two surfaces of the tweezers together (based on perception of the test conductor). Images were taken before and after each set of crimps. Thermal performance testing was conducted between each defect level as defined in Table 5.

b. Cut Testing Description

Cut testing was performed similarly to Crimp testing with the exception that defects were produced by using a surgical knife to cut through individual fibers. Fibers were selected at the center of the fixture and the outside edge of the fiber bundle. Fixtures 5 and 6 from the Critical Characteristics testing were reused for Cartridge 2 and 3, respectively. In addition to thermal performance testing, the accumulated water on the shell side of the test stand was captured and the volume estimated.

c. Hydrophobicity Testing Description

Hydrophobicity testing was conducted in three phases. In Phase 1, exploratory testing on stand-alone membranes (unassembled) was conducted to determine the effect of surfactant exposure to membrane hydrophobicity. Non-ionic Triton X-100 was used as the challenge surfactant analog for dimethylsilanediol, which has been shown to be a known surfactant in ISS water systems.[10] The test was conducted by first cutting a hollow fiber membrane along the axial length using a Feather incision knife and flattening on a piece of double sided tape. Tweezers were used to press the ends of the tube flat on the surface (without touching the area to be tested) with the outer wall of the tube facing up. A baseline contact angle of deionized water was measured using a goniometer. A droplet of Triton X-100 solution was then placed on the membrane in a designated location and allowed to sit for 1 minute. A contact angle measurement was then taken again. The membrane material was exposed to Triton X-100 concentrations of 0.25 vol%, 0.5%, 0.75%, and 1% without rinsing between tests.

Phase 2 was designed to evaluate the effect of decreased contact angle on assembled SWME membrane modules. Because the internal lumen contact angle of an assembled SWME module could not be determined, Phase 2 took a parallel approach in which stand-alone membranes (unassembled) and SWME modules were exposed to identical conditions. The assumption was made that the observed change in contact angle of the unassembled membrane would be approximately equal to the internal contact angle of the assembled SWME module. To save test time, Phase 2 performance checks of each cartridge were conducted at a single condition: 32.7 mL/min water flow at 24 psia, 19°C inlet temperature, and ALARA shell pressure. To begin, the baseline performance of each module (Cartridges 4, 6, and 8) was determined. Next, the modules were exposed to a solution of Triton X-100 by gravity flowing through the cartridge for 10 minutes followed by gravity rinsing with deionized water for 30 minutes. After Triton X-100 exposure, a performance check was conducted of the module. Once complete, the module was removed from the test stand and exposed to the next solution of Triton X-100. All tests of a given cartridge were completed in a single day. Table 6 describes the concentrations of Triton X-100 exposed to each cartridge during Phase 2.

Table 6. Phase 2 hydrophobicity testing surfactant challenge concentrations.

Cartridge	Triton X-100 Level 1	Triton X-100 Level 2	Triton X-100 Level 3
4	0.25%	0.75%	N/A
6	0.25%	0.75%	0.75%
8	0.75%	N/A	N/A

Phase 3 was designed to evaluate the cumulative effect of surfactant on a given cartridge. Cartridge 4 was used in Phase 3. After its exposures in Phase 2, the cartridge was subsequently exposed to concentrations of 0.75%, 1.25%, 1.75%, and 2.25% Triton X-100 using the same method as Phase 2. Performance checks were conducted between each exposure and included a full sweep (7-10 discrete values) of pressures beginning at ALARA. Because the test occurred over multiple weeks, Baseline performance tests were conducted and baseline contact angle measurements were taken prior to each new exposure.

III. Results and Discussion

A. Critical Characteristic Testing Results and Discussion

Three membranes with unique critical characteristics were chosen to evaluate the effect of those characteristics on heat rejection performance. Figure 4 shows both the raw empirical data (data points) and the model predicted values (lines) for lumen temperature difference ($dT = T_{in}-T_{out}$), normalized by multiplying by the flow rate versus the

evaporation driving force (ΔP). To estimate the value of S_p, a least squares regression was performed to minimize the difference between predicted and experimental temperature change for the data obtained with each module. A parity plot (Figure 5) shows the relative agreement of the experimental vs the calculated (model-predicted) values for lumen temperature difference. This data provides validation of the defined models and verifies the quality of data collected in the test stand over the ranges shown.

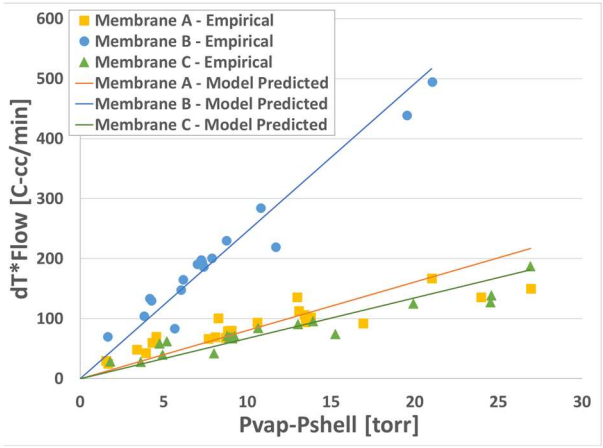

Figure 4. Empirical data compared to model predictions for lumen temperature differences vs driving force.

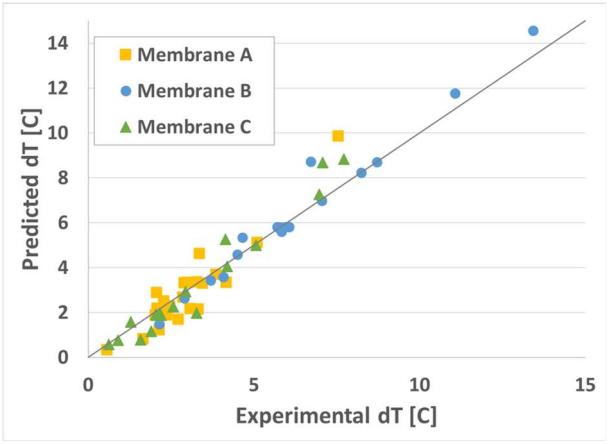

Figure 5. Parity plot for experimental vs predicted lumen temperature difference.

B. Contamination Testing Results and Discussion

Ersatz mixtures for contamination testing were prepared within 24 hours of beginning each test in the Recirculation Test Stand. Conductivity and pH measurements were taken of the fresh ersatz. Notably, the pH and conductivity were strongly a function of the inorganic contamination concentration (pH data shown in Figure 6), with the High level of inorganics resulting in the highest values of pH, iron precipitation, and conductivity. Organic contamination contributed slightly to the measured pH with lower organics resulting in slightly higher pH, though did not seem to affect conductivity. Finally, the presence of iodine biocide generally increased the overall pH of the ersatz relative to mixtures without biocide.

Two levels of microbial concentrations were targeted as described above. The actual microbial concentrations of the ersatz varied as shown in Figure 7.

Twenty-eight test runs were planned as shown in Table 3. Each was planned to run for a total of 20 days

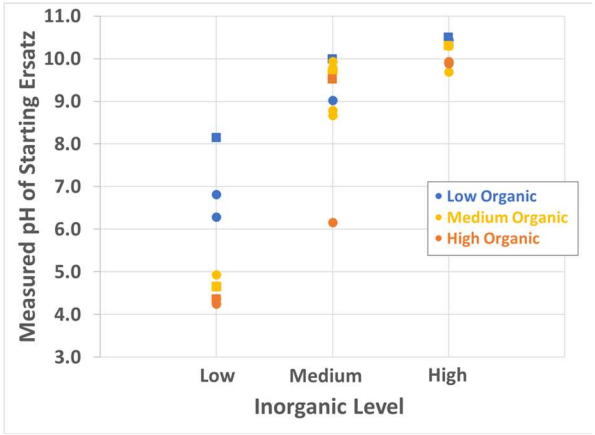

Figure 6. Starting pH of ersatz mixtures for Contamination Testing runs. *Square data points denote biocide present in the ersatz.*

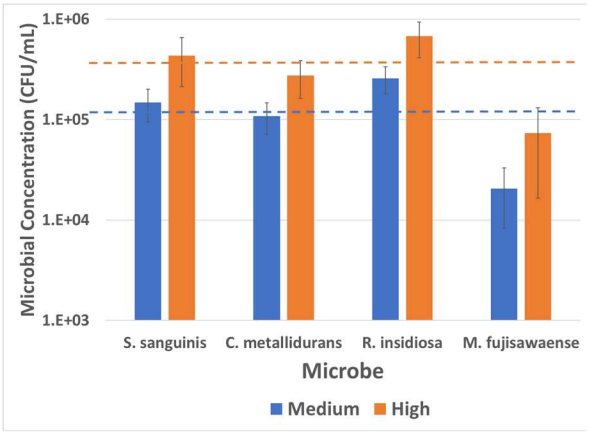

Figure 7. Average microbial concentration in ersatz for Contamination Testing at Medium and High organic levels. *Error bars indicate one standard deviation. Dashed lines indicate targeted concentration for Medium (blue) and High (orange) microbe counts.*

with performance checks approximately half-way through and at the end the run. Three tests were inadvertently stopped a day early at 19 days (Fixtures 7, 9, and 10). Three of the tests were intentionally stopped prior to the full 20 days. Fixtures 1 and 11 were stopped after 6 and 8 days, respectively, due overpressure of the lumen side. Post-test inspection of the fiber inlet showed significant contamination of the cross-section, as shown in Figure 8. Analysis determined the contamination to be iron oxides from the ersatz solution. Fixture 12 was stopped after day 10 due to a leak in the plastic housing of the cartridge, believed to be caused by overtightening of metal national pipe taper (NPT) fittings to the plastic. Fixture 16 was run the full duration in the Recirculation Test Stand, but thermal check data are not available for the end of the test due to the test being inadvertently run with no vacuum applied to the shell side. All other Fixtures were tested to completion and data collected without issue.

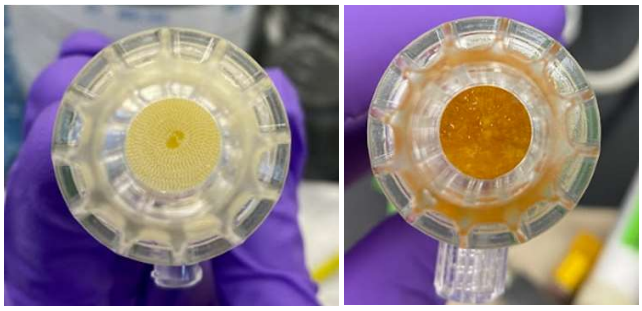

Figure 8. Fixture 1 lumen inlet prior to contamination testing (left) and after 6 days of contamination testing (right). *Contamination was determined to be iron oxide precipitate occluding the fiber inlet and causing increased pressure drop across the lumen.*

No significant change was observed in either pH or conductivity of the ersatz solutions over the duration of the Contamination testing. For mixtures containing high quantities of biocide (4 ppm iodine), no microbes were observed at the end of the test with the exception of when M. *fujisawaense* was also initially a high quantity (Fixture 21) and for R. *insidiosa* where no microbes were intentionally introduced into the challenge mixture (Fixture 27). This can only be explained by contamination, though it is not clear if the contamination was in the challenge test or in the post-test microbial analysis. Microbial growth was observed in several cases where no microbes or biocide were initially introduced, suggesting contamination (C. *metallidurans* in Fixtures 5, 13, 17; R. *insidiosa* in Fixtures 5, 13, 14, 16, and 17; and M. *fujisawaense* in Fixtures 5, 14, and 16). For Fixtures 26 and 27, no microbes were intentionally added to the challenge mixture but 4 ppm of biocide was added. Despite the biocide, microbes were observed at day 19, though they did not match the challenge microbes, again suggesting contamination. All other fixtures generally showed a decrease in microbial counts at day 19 compared with the test start, regardless of the quantity of biocide added. No biofilms were observed in any of the fixtures or test stand hardware post-test.

Heat rejection from the cartridge can be observed as a temperature drop across the lumen (T_{in}-T_{out}) during operation. The driving force is the difference between the vapor pressure of the water and the shell side vacuum pressure (P_{vapor}-P_{shell}). While the inlet temperature for all performance check testing was approximately 30ºC, maintaining a constant shell pressure was more difficult due to the capability of the vacuum pump. To provide a comparison of the data, we plot the change in temperature across the lumen (dT) multipled by the water flow rate through the cartridge (50 mL/min) versus the driving force where we expect to see a linear relationship across a range of P_{vapor}-P_{shell} values. On Day 1 of all testing, a baseline performance test was conducted. All the starting values are expected to be approximately the same since they were all run with new cartridges under similar conditions. The variation observed in the Day 1 data can then be attributed to the inherent variability of the cartridges. Figure 9 shows all Day 1 experimental cartridge data matches closely with the modeled data. It should be noted that heat rejection is directly related to the mass of water vaporized, which in turn is a function of inlet temperature and the pressure differential driving force.

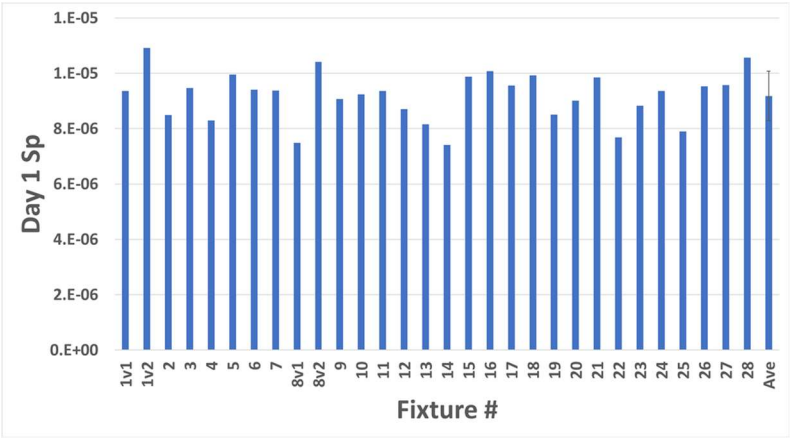

Figure 9. Day 1 Sp values for all fixtures. *"Ave" represents the average Sp value of all fixtures on day 1. Error bar indicates standard deviation. Note that the first run attempt for Fixtures 1 and 8 (1v1, 8v1)resulted in a mechanical failure such that new Fixtures were used to restart the tests.*

Thermal performance checks were conducted mid-way through and

at the end of each contamination challenge test. Fixtures 3, 4, 8, 9, and 15 were exposed to identical conditions (Medium Organics, Medium Inorganics, and Low Biocide). The ratio of the driving force to the measured temperature drop at a given flow rate (ΔP/dT*Flow) can be used as an initial gauge of membrane degradation. Figure 10 shows the change ΔP/dT*Flow as a function of days exposed to contamination ersatz and Fixture number. As can be seen, there was a reduction in performance observed for all fixtures except Fixture 15, which was approximately flat (though not clear why). A similar observation was made in a previous study[3] where the SWME membrane was challenged for three days with 33 EVA, 66 EVA, and 100 EVA equivalent concentration of contaminants. Over 3 days, the test observed a 0.54% decrease in heat rejection performance. This study shows ~6.5% reduction in performance over 7-10 days at ~25 EVA equivalent concentration of contaminants.

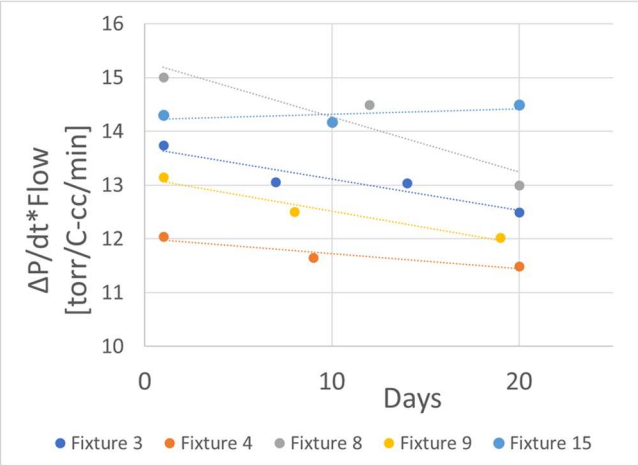

Figure 10. Reduction in performance as a function of time and Fixture under idential contamination exposure conditions.

A statistical analysis of the data was conducted to determine which factors had significant influence on membrane performance as demonstrated by a change in S_p. Several fixtures were excluded from the analysis for reasons described in Table 7. Statistical power is the probability that a statistical test makes a correct conclusion and effects are detected when they exist. For example if the truth is that the level of Inorganics changes S_p, power is the probability that the statistical test will conclude that inorganics has a significant effect on S_p. Statistical rule of thumb is to have statistical power ≥ 0.8. For the as-run test matrix, Inorganics, Organics, and their interaction had statistical power ≥ 0.8. However, the as-run test matrix has low power for Biocide individual effect and interactions involving Biocide. This means that there may be cases where Biocide has an effect or an interaction effect that the statistical test did not detect. More testing would be needed to have confidence in the presence or lack of Biocide and interaction effects.

Table 7. Data excluded or partially included in statistical analysis.

Fixture #	Data Available	Exclude Data?	Notes
1	None	Exclude	Increased water pressure on lumen side due to iron precipitate. Testing discontinued.
10	All	Exclude	Leak due to crack in housing that caused air leak into system during testing and resulted in higher PT3. Never reached steady state.
11	None	Exclude	Crack on inlet allowed water leakage. Leak caused by iron precipitate which reduced flow through fibers and increased pressure. Testing discontinued.
12	Days 1-10	Exclude	Crack on inlet caused leakage. Testing discontinued.
16	Days 1-10	Exclude	Leak due to kink in tubing at pump head. Solution was remade and restarted on Day 6. Forgot to turn on vacuum, so performance data for last day of test not available.
3	All	Include, but some missing	Fixture 3 is included in the dataset; however, data on the amount of bacteria is missing.

The statistical analysis showed (90% confidence) that Inorganics, Organics, and time all reduced S_p, as shown by the plot in Figure 11. While the specific critical membrane characteristics that are changing have not been confirmed, observations from the test may provide some clue. First, as mentioned above, precipitation of iron oxide was observed in cartridges with high Inorganic. It is plausible that small quantities of the precipitate deposited along the inner lumen walls, thereby reducing the effective porosity and pore diameters within membrane. For Organics, no biofilm formation was observed on any of the modules. However, it is possible that individual microbes could have adhered to the internal lumen surfaces, again reducing the effective porosity and pore diameters within the membrane. Finally, time is shown to result in a decrease in S_p. Polypropylene membranes are noted for their robustness to chemical degradation. Further, the test exposure time did not exceed 20 days, much shorter than the duration these types of materials are used in industry. As such, this observed decrease in S_p with time is likely to be a function of duration of exposure of the chemicals rather than a result of natural change in the membrane over time.

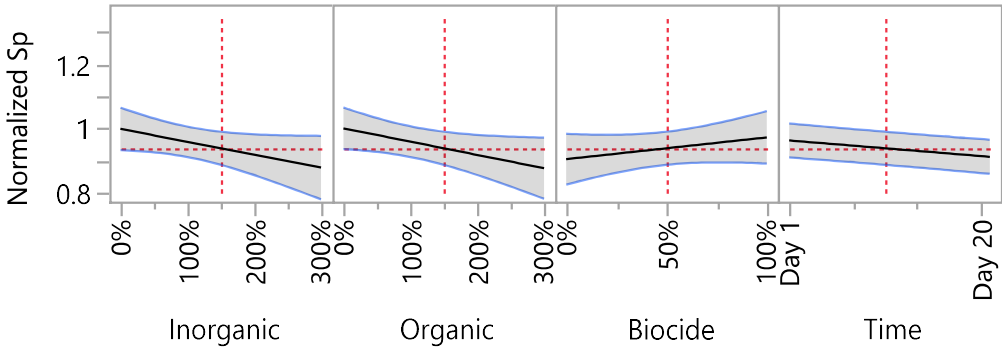

Figure 11. Plot showing the effects of Time, Inorganic levels, Organic levels, and Biocide on Sp.

C. Defect Testing Results and Discussion

1. Crimp Testing results

Crimp testing was the first of the defect tests to be conducted. Microscopic images of the crimps, as shown in Figure 12, indicate relatively uniform crimping. Thermal performance checks were conducted immediately following the crimping of the fibers. A significant and predicable increase in pressure drop was observed between 5 and 20 crimps. A corresponding decrease in thermal performance was also observed, providing further evidence that available surface area for vaporization was decreased. Unexpectedly, when 50 crimps were applied, the pressure drop returned to values consistent with 5 crimps. One possible explanation is the location of the crimps in the cartridge. For crimps 5-20, all crimps were along one side of the cartridge, each on a separate fiber. This flow resistance would have reasonably provided a concentrated force such that the water flow simply increased to the other (uncrimped) fibers in the cartridge. When crimps 21-50 were applied, there was no additional space on the first side of the cartridge. Therefore, the crimps were applied exactly opposite the cartridge. It is possible that the even distribution of the crimps were sufficient to balance the restrictive force and allowed the flow to be more evenly applied across the membranes, helping to partially "uncrimp" the fibers. Attemps were made to determine if the crimps relaxed to reopen the fibers, however, no change could be measured with the available microscope. Ultimately, these data show that even a partial restriction (e.g. mechanical damage to the fibers, partial obstruction, etc.) of as few as 0.8% of the fibers, will result in increased pressure drop across the lumen side. This corresponds to approximately 77 fibers in a single SWME module. A statistical analysis showed S_p was not affected by crimping. The only critical characteristic that might be affected by crimping would be wall thickness. However, for the surface area with decreased wall thickness relative to the entire the membrane surface area, the impact may be too small to observe in the current test. The only statistically significant effect was on lumen

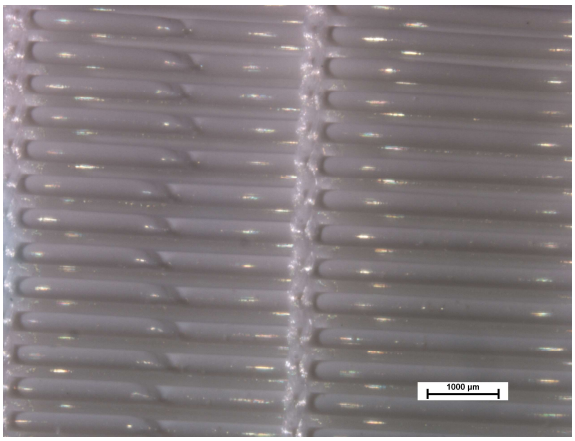

Figure 12. Crimp defect testing showing crimps 1-20.

inlet pressure ($p<0.05$). This is to be expected as a decrease in total cross section flow area would result in backpressure on the system. The lumen outlet temperature (T_{out}) was nearly statistically significant ($p=0.0523$) and would be expected to be affected due to the increased velocity of water through the lumen. Similarly, the total heat rejection ($p=0.1335$) would be expected to decrease due to the effective decrease in lumen diameter per Equation 1. Additional testing could be used to increase the data from which the analysis is conducted and destructive post-analysis of the fibers might be used to evaluate the change in diameter.

2. Cut Testing Results

Two fixtures were tested to observe the effect of fibers being cut. The original test plan had 0, 1, 2, 5, and 10 fibers cut with performance checks between. However, in both cases, the data showed that with a single fiber cut, sufficient liquid water entered the shell side prior to initiating vacuum, that the vacuum pump had to cyclically pump out the liquid, thereby temporarily losing vacuum. During the loss of vacuum, the temperature of the membrane would increase, partially thawing the membrane, and additional liquid would enter the shell side. This cycle occurred a total of three times for both membranes before the system achieved a steady-state. A graph showing this phenomenon for one of the fixtures is shown in Figure 13. Notably the vacuum, when achieved, was sufficiently low for sublimation to occur (~5 torr). Depending on the intravehicular cooling loop design and startup operation for a future spacesuit, there is potential for liquid water to enter the shell side prior to full vacuum. If this then partially or fully blocks the vacuum control valve, the cyclic freeze/thaw may be observed. Testing here shows that this is a recoverable failure, though intermediate thermal control may be compromised. Additional cuts (beyond 1 cut) were not tested in this study in order to protect the vacuum pump. Future testing would benefit from an evaluation to determine the "break point" of numbers of cut fibers from which there is no recovery.

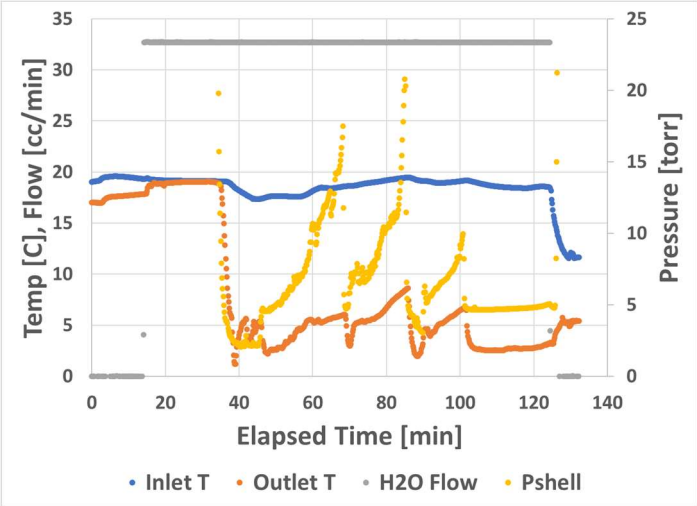

Figure 13. Cut test data showing cyclic loss of vacuum followed by steady-state sublimation.

3. Hydrophobicity Testing Results

Hydrophobicity testing was conducted in three phases. Each phase yielded important data for the subsequent phases as described below.

Phase 1 Hydrophobicity Testing

Phase 1 test data provided two pieces of information used in the remaining testing. First, it demonstrated the variability of the raw membrane contact angle. It is not clear if this variability is due to the goniometer method itself or real differences in local surface energy of the membrane. Regardless, the untreated membrane had an overall average contact angle measurement of 116° with a standard deviation of 4°. This is slightly higher than the reported 110° contact angle of this type of membrane. Second, testing showed that small increases in the concentration of Triton-X-100 resulted in measurable differences in contact angle of the membrane, as seen in Figure 14. Accordingly, 0.25% Triton X-100 was chosen as a starting point for cartridge exposure in Phase 2, with small increases to prevent instantaneous wetout of the membranes.

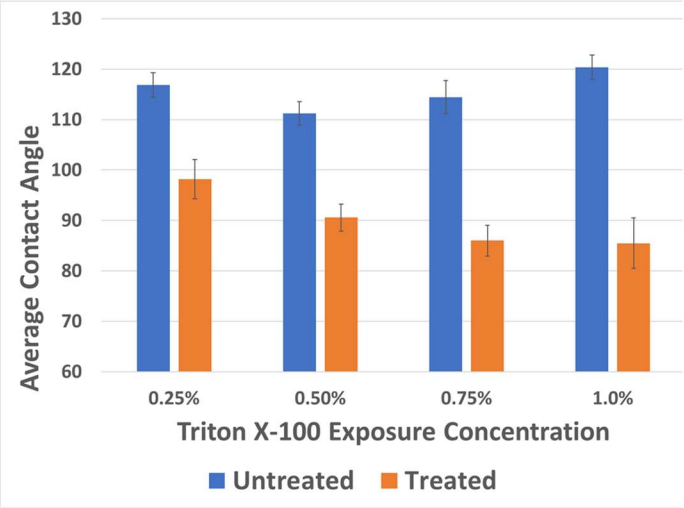

Figure 14. Effect of Triton X-100 concentration on contact angle of hollow fiber membranes.

Phase 2 Hydrophobicity Testing

Surfactant is known to decrease the surface energy of the membrane. This results in increased water entry into the pores and a corresponding decrease in effective membrane thickness. As effective membrane thickness decreases, S_p will increase and the slope of the performance vs driving force correlation will increase. Figure 15 shows the performance vs driving force results for Phase 2 hydrophobicity testing. The triangles show baseline performance for Cartridge 4 (C4), Cartridge 6 (C6), and Cartridge 8 (C8). As expected, the curves are very similar and differences can be attributed to slight differences in the cartridges themselves (i.e. actual number of fibers, variability between lots of fibers, variability of porosity and pore size across membranes, etc.). The circles and diamonds show performance following exposure to Triton X-100 for C4 and C6, respectively. The data showed that exposure to the 0.25% Triton X-100 had negligible effect on either cartridge. All of the cartridges were exposed to 0.75% Triton X-100 and each showed a different effect. When C4 was subsequently exposed to 0.75% Triton X-100 (filled blue circle), a significant change in performance was observed as indicated by the increase in the slope of the line. However, when C6 was exposed to 0.75% Triton X-100 (dark green diamond), very little change was observed. There were no differences in procedure for this test and the same Triton X-100 solution was used for both Cartridges. However, when evaluating the contact angle on the unassembled membrane for the two tests, a significant difference was observed. The water contact angle on the unassembled membrane for C4 after exposure to 0.75% was 80.2° while the contact angle for C6 after exposure to the same 0.75% solution (albeit 24 hours later) was 93.2°. While it is not clear why this difference was observed, the unassembled membrane data and the performance vs driving force data make sense if we assume the internal contact angles of the cartridges were similar to the unassembled membrane. One theory is that the Triton X-100 solution was not fully mixed before application to C6. Regardless, a new 0.75% Triton X-100 solution was mixed and applied to the unassembled membrane and C6. The light green diamond shows the performance after this exposure and an increase in slope is observed. As expected, the slope of the line increases as the effective wall thickness decreases and S_p increases. Finally, C8 was exposed to 0.75% Triton X-100 several weeks after the other two cartridges. A new solution was used for the treatment. The cartridge wetted out immediately and thermal performance data could not be collected. Notably, the measured contact angle on the unassembled membrane for the C8 test was only 76.7°. Other membranes (data from Phase 3 discussed below) with similar contact angle did not exhibit wetout.

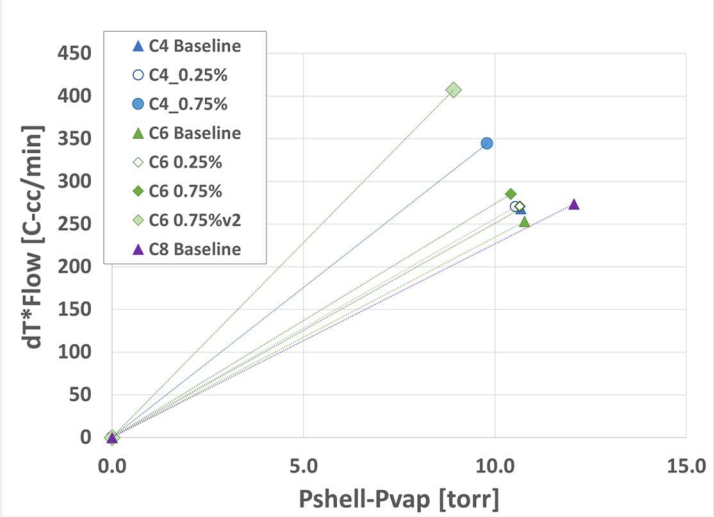

Figure 15. Performance vs driving force results for Phase 2 hydrophobicity testing.

Phase 3 Hydrophobicity Testing

Cartridge 4 was used for Phase 3 testing. Several observations were made. First, as expected, repeated exposure to increasing concentrations of Triton X-100 resulted in continuous decrease in contact angle of the membrane. Unexpected, however, was that between treatments, the membranes seemed to partially recover their hydrophobicity. Figure 16 shows all contact angle measurements on the unassembled membranes. The "Baseline" (B#) contact

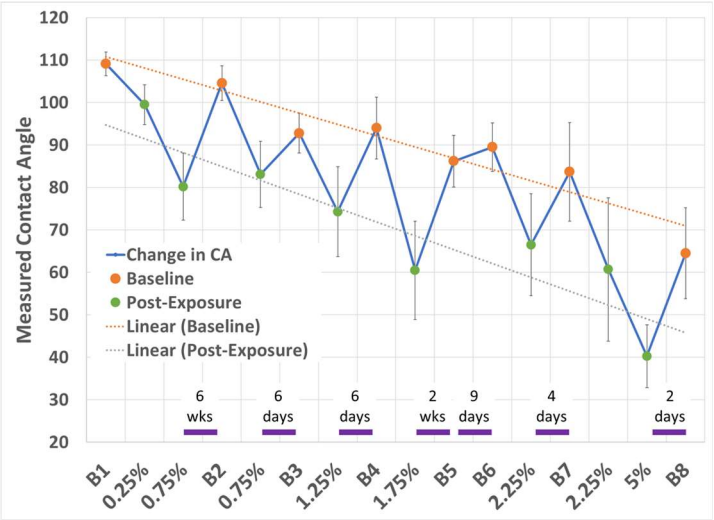

Figure 16. Phase 3 baseline and post-exposure contact angle measurements.

angle was measured at the start of a test day on the dry membrane before Triton X-100 was administered. The measurements labeled with concentrations were taken following Triton X-100 exposure. Measurements are shown in the order they were taken (left to right). Purple lines show the durations the unassembled membranes and cartridge sat dry between samples. It is not clear why the partial recovery of contact angle was observed. If flow of water during performance checks was able to flush out residual Triton X-100 at the pores, then performance of the cartridge would be expected to look similar to baseline performance. However, as can be seen in Figure 17, performance checks showed that the slope of performance vs driving force was greater than baseline performance for every test sequence. This suggests that for the entirety of the performance check after Triton X-100 exposure, the membrane remained less hydrophobic. This then implies that the recovery of the contact angle/surface energy occurred following the test, potentially when the membrane and cartridge were stored dry. Triton X-100 has a very low vapor pressure (<1 mmHg at 20°C) and would not be expected to have significant evaporation from the membrane over the duration between tests. Another theory is that the Triton X-100 remained on the surface but migrated, either into the membrane polymer matrix, or through the pores and onto the external surface of the fibers. Neither theory could be confirmed.

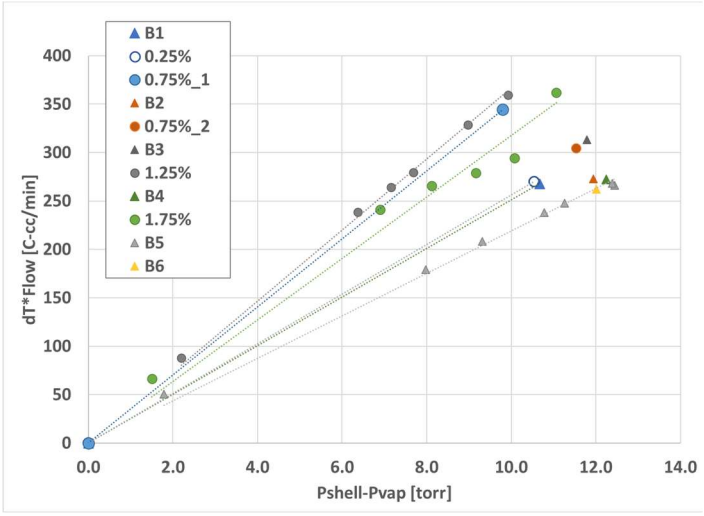

Figure 17. Observed change in performance vs driving force curves between baseline and treated performance checks.

For all contact angles <75°, full wet out of the membrane was observed. In these cases water froze along the external length of the fibers as seen in Figure 18. This data shows that for low concentrations of surfactant, performance of the cartridge will appear to improve. However, at a critical surface energy, the membrane will fully wet out. No additional effort was made here to recover performance of the fully wetted cartridge. Future testing will look at a variety of recovery methods for this scenario. Additionally, the membrane tested here had a wall thickness of 48 nm. Membranes with thinner walls would be more susceptible to wet out because the time to reach the critical point (wherein the Kundsen diffusion layer exceeds the vapor thickness layer) would occur more rapidly. Additionally, repeated exposure to surfactant will gradually decrease hydrophobicity, but periods of dry out may partially recover performance.

Figure 18. Water frozen along external length of Cartridge 4 following full wet-out.

IV. Conclusions and Future Work

Real-time failure prediction of the SWME would provide significant risk reduction for Lunar and Martian surface operations where the portable life support system is reused and may encounter both gradual and instantaneous degradation. The results reported here provide the initial validation data for these types of models wherein insight into water flow rate, inlet and outlet lumen temperatures, and shell pressure can be used to continuously monitor the "health" of the membranes. Trends in performance changes can then be attributed to specific failure mechanisms such as surfactant exposure, particulate contamination, and/or microbial contamination. Next steps will involve completion of the contamination and defect testing and a concentrated effort to build the grounded model for operational surveillance of the SWME in a flight environment.

Acknowledgments

The authors would like to acknowledge the members of the SWME Risk Mitigation Assessment Team who provided substantial technical contributions, but were unable to author sections of this paper including Lora Bailey and Rodney Rocha for vibe testing, Dr. Gene Ungar for thermal analysis support, Drs. Mary Hummerick, Misle Tessema, Carolina Franco, and Athela Frandsen for their support in ersatz preparation and analysis, and Colin Campbell for his guidance on this project.

References

[1] Vogel, M., Peterson, K., Zapata, F. III, Dillon, P., Trevino, L. A., "Spacesuit Water Membrane Evaporator Development for Lunar Missions," SAE 2008-402-0313, 38th International Conference on Environmental Systems, June 29-July 2, 2008, San Francisco, CA.

[2] Harris, B., Leimkuehler, T.O., Fricker, J., "Development of a Back Pressure Valve for the Spacesuit Water Membrane Evaporator (SWME)," ICES-2015-338, *45th International Conference on Environmental Systems*, July 12-16, 2015, Bellevue, WA.

[3] Bue, G.C., Trevino, L.A., Tsioulos, G., Settles, J., Colunga, A., Vogel, M., Vonau, W., "Hollow Fiber Spacesuit Water Membrane Evaporator Development and Testing for Advanced Spacesuits," AIAA-2010-6040, *40th International Conference on Environmental Systems*, July 11-15, 2010, Barcelona, Spain.

[4] Bue, G.C., Makinen, J., Vogel, M., Honas, M., Dillon, P., Colunga, A., Truong, L., Porwitz, D., Tsioulos, G., "Hollow Fiber Space Water Membrane Evaporator Flight Prototype Design and Testing," *41st International Conference on Environmental Systems*, AIAA-2011-5259, *41st International Conference on Environmental Systems*, July 17-21, 2011, Portland, OR.

[5] Bue, G. C., Makinen, J., Cox, M., Watts, C., Campbell, C., Vogel, M., Colunga, A., and Conger, B., "Long-Duration Testing of a Spacesuit Water Membrane Evaporator Prototype," AIAA-2012-3459, 42nd International Conference on Environmental Systems (ICES), San Diego, CA, July 2012.

[6] "NASA Partners with Industry for New Spacewalking, Moonwalking Services," https://www.nasa.gov/news-release/nasa-partners-with-industry-for-new-spacewalking-moonwalking-services/, accessed February 12, 2024.

[7] Khan, M.,A., Lipscomb, G., Lin, A., Baldridge, K.C., Petersen, E.M., Steele, J., Abney, M.B., Bhattacharyya, D., "Performance evaluation and model of spacesuit cooling by hydrophobic hollow fiber-membrane based water evaporation through pores," *Journal of Membrane Science*, 2023 (In Press).

[8] Hansen, C., Cassidy, C., "Mishap Investigation Board Summary of Extravehicular Activity 23: Lessons Learned from a Spacewalk Close Call," *Journal of Space Safety Engineering,* vol. 1, iss. 1, June 2014, pgs 32-39.

[9] Westheimer, D., Campbell, C., Contreras-Baker, A., Steele, J., "SERFE Water Quality Results," ICES-2022-285, *51st International Conference on Environmental Systems*, July 10-14, 2022, St. Paul, MN.

[10] Perry, J.L., Kayatin, M.J., "The Incidence and Fate of Volatile Methyl Siloxanes in a Crewed Spacecraft Environment," ICES-2017-233, *47th International Conference on Environmental Systems*, July 16-20, 2017, Charleston, SC.